Annals of Nuclear Energy 87 (2016) 500–510

Contents lists available at ScienceDirect

Annals of Nuclear Energy

journal homepage: www.elsevier.com/locate/anucene

Ultimate analysis of PWR prestressed concrete containment under long-term prestressing loss

Hsuan-Teh Hu [1], Jun-Xu Lin [1]

National Cheng Kung University, Tainan 701, Taiwan, ROC

ARTICLE INFO

Article history:
Received 21 August 2014
Received in revised form 5 October 2015
Accepted 7 October 2015

Keywords:
Ultimate analysis
Prestressed concrete containment
Prestressing loss

ABSTRACT

Numerical analyses are carried out by using the Abaqus finite element program to predict the ultimate pressure capacity and the failure mode of the PWR prestressed concrete containment at Maanshan Nuclear Power Plant, Taiwan, R.O.C. under long term prestressing loss. Material nonlinearity such as concrete cracking, tension stiffening, shear retention, concrete plasticity, yielding of prestressing tendon, yielding of steel reinforcing bar, yielding of liner plate and relaxation of prestressing tendon are all simulated with proper constitutive models. The results of the numerical analysis show that after the 40 years of service, the prestresses in the prestressing tendons would lose about 19% of their initial values. However, under long term prestressing loss, the ultimate pressure capacity of the containment is still higher than the design pressure 482 kPa by 58%.

1. Introduction

Since the accident at Three Mile Island nuclear plant in 1979, it has become necessary to perform failure analysis and calculate the ultimate pressure capability of the nuclear reactor containment for the safety assessment of nuclear power plants (U.S. Nuclear Regulatory Commission, 1987; Amin et al., 1993; Boeck, 1993). The containment structures in service at Taiwan, R.O.C. were built in the late 70's or early 80's. Since then, nonlinear material constitutive models and nonlinear finite element solution techniques have been continuously and successfully developed (Argyris et al., 1974; Connor and Sarne, 1975; Goodpasture et al., 1978; ASCE, 1982; Chen, 1982; Meyer and Okamura, 1985; Hu and Schnobrich, 1989, 1990; Borri and Sorace, 1993; Smith, 2001). Therefore, it is possible to predict the ultimate pressure capability of the nuclear reactor containment more accurately than before by utilizing the nonlinear finite element method (Pfeiffer et al., 1992; Andreoli et al., 1993; Saito et al., 1993; Hu and Liang, 2000; Basha et al., 2003; Hu and Lin, 2006; Abaqus, 2007).

The Atomic Energy Council at Taiwan, R.O.C. has run several studies toward the failure analysis of containment structures. As one of the research projects sponsored by AEC, the aim of this paper is to employ the nonlinear finite element program Abaqus (Dassault Systèmes Corporation, 2014) to investigate the ultimate pressure capacity and the failure mode of the PWR (Pressurized Water Reactor) prestressed concrete containment at Maanshan nuclear power plant, Taiwan, R.O.C. under long-term prestressing loss.

Long-term prestressing loss is a major cause of concern for prestressed concrete containment structure (Smith, 2001; U.S. Nuclear Regulatory Commission, 1990; Cornish-Bowdena et al., 2011). Information available on prestressing loss of a number of US, French and Russian containment structures indicates that relaxation of prestressing cables along with creep and shrinkage of concrete caused high long term prestressing loss as compared to the estimated loss at the time of design (Ashar et al., 1997; Maliavine, 1997; Martinent et al., 1997; Patel et al., 2007). In addition, it shows that higher prestressing losses of the US plants was attributed, mainly to higher relaxation of the prestressing steel and to a lesser extent to creep and shrinkage of concrete (Patel et al., 2007). Since the PWR prestressed concrete containment at Maanshan nuclear power plant follows the design standards of US, the focus of this investigation is on the long-term prestressing loss due to the relaxation of the prestressing steel tendon. As the result, creep and shrinkage of concrete are not considered in this investigation.

In the paper, the geometry and finite element mesh of the containment are reviewed first. Then, material properties of reinforcing steel bar, liner plate, prestressing tendon and concrete are given and proper constitutive models are introduced to simulate the nonlinear behavior of these materials such as yielding of reinforcing steel bar, yielding of liner plate, yielding of prestressing tendon, relaxation of prestressing tendon, concrete cracking, tension stiffening, shear retention, and concrete plasticity. Finally, failure

[1] Department of Civil Engineering.

http://dx.doi.org/10.1016/j.anucene.2015.10.005
0306-4549/

analyses of the containment under long-term prestressing loss and subjected to internal pressure are carried out and important conclusions are given.

2. Containment geometry and finite element mesh

The PWR prestressed concrete containment at Maanshan Nuclear Power Plant is composed of a circular base slab, an upright cylinder and a hemispherical dome (Fig. 1). To simplify the analysis, the tendon gallery, equipment hatches and penetrations on the containment are not considered and the structural geometry is assumed to be axisymmetric. The base slab of the containment is embedded in the soil and the dimensions of the containment are given in Fig. 1.

The entire interior surface of the dome, cylinder and base slab are lined with continuous steel plate of 0.635 cm thickness to provide a leak-tight barrier. At the cylinder wall, the prestressing tendons are placed in the meridian and circumferential directions of the containment. At the dome, the prestressing tendons are placed in the circumferential direction and the directions parallel to x and y coordinates (Fig. 2a). Most of the steel reinforcing bars are placed in an axisymmetric manner in the containment but some steel reinforcement layers near the apex of the dome and in the base slab are placed in the directions parallel to x and y axes. The detailed arrangements of prestressing tendons and steel reinforcing bars are given in the Final Safety Analysis Report of the Maanshan nuclear power plant (Taiwan Power Company, 1981). Because some prestressing tendons and some steel reinforcing bars are not placed axisymmetrically, the deformation of the containment is no longer axisymmetric and has four planes of symmetry (Fig. 2a). As a result, only 1/8 part of the structure is analyzed and the boundary conditions imposing on the symmetric planes are displacements in the circumferential direction, rotations in the radial direction and rotations in the z direction to be zero. For simplicity, the lateral pressure applied to the base slab due to soil is not considered.

In the numerical simulation, 8-node shell elements (six degrees of freedom per node) with reduced integration rule are used to model the parts of dome and cylinder, and 27-node solid elements (three degrees of freedom per node) with reduced integration rule are used to model the base slab (Fig. 2b). The steel liner plates at the parts of dome and cylinder are modeled by the 8-node shell elements with reduced integration rule and the liner plates at the top of the base slab are modeled by the 9-node shell elements with reduced integration rule. Those steel liner plates are either linked to the shell elements of the concrete section (assuming no offset) at the parts of dome and cylinder, or attached to the inner surface of the solid elements at the top of the base slab. The formulation of the shell elements allows transverse shear deformation

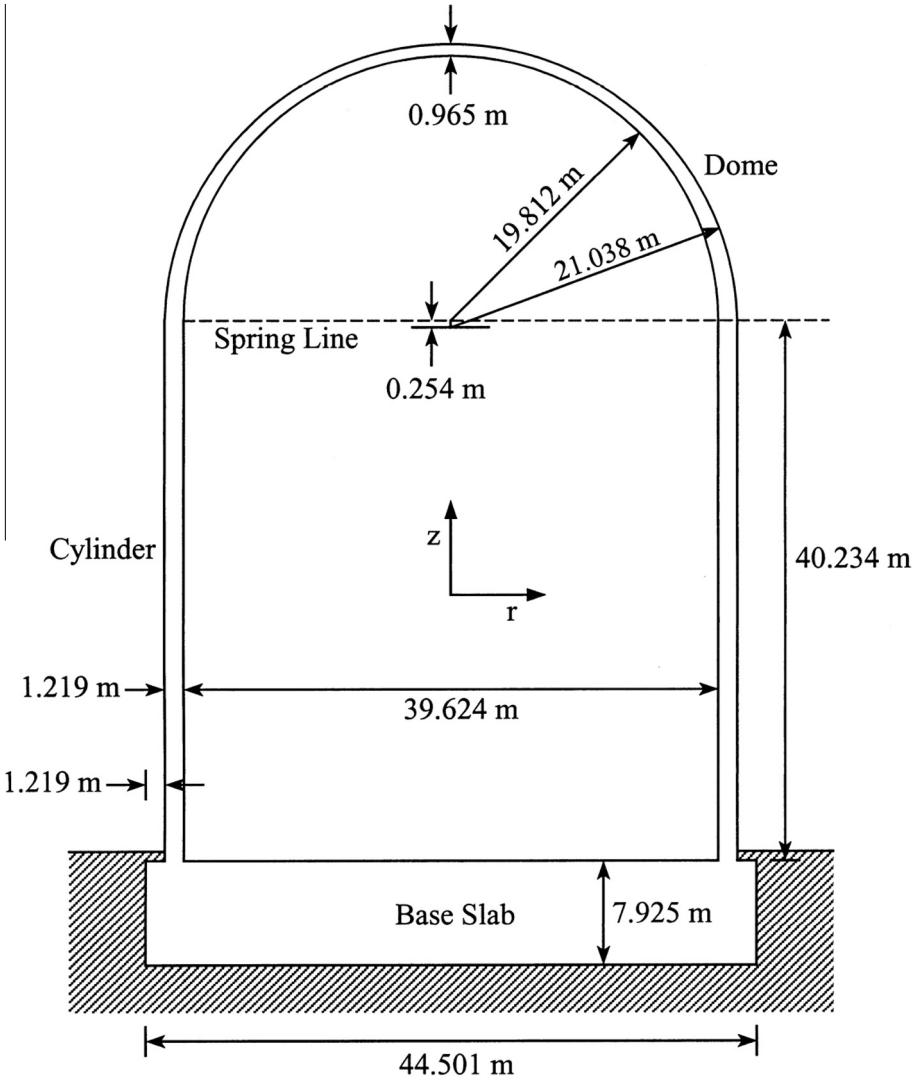

Fig. 1. Geometry and dimensions of the PWR prestressed concrete containment of Maanshan nuclear power plant.

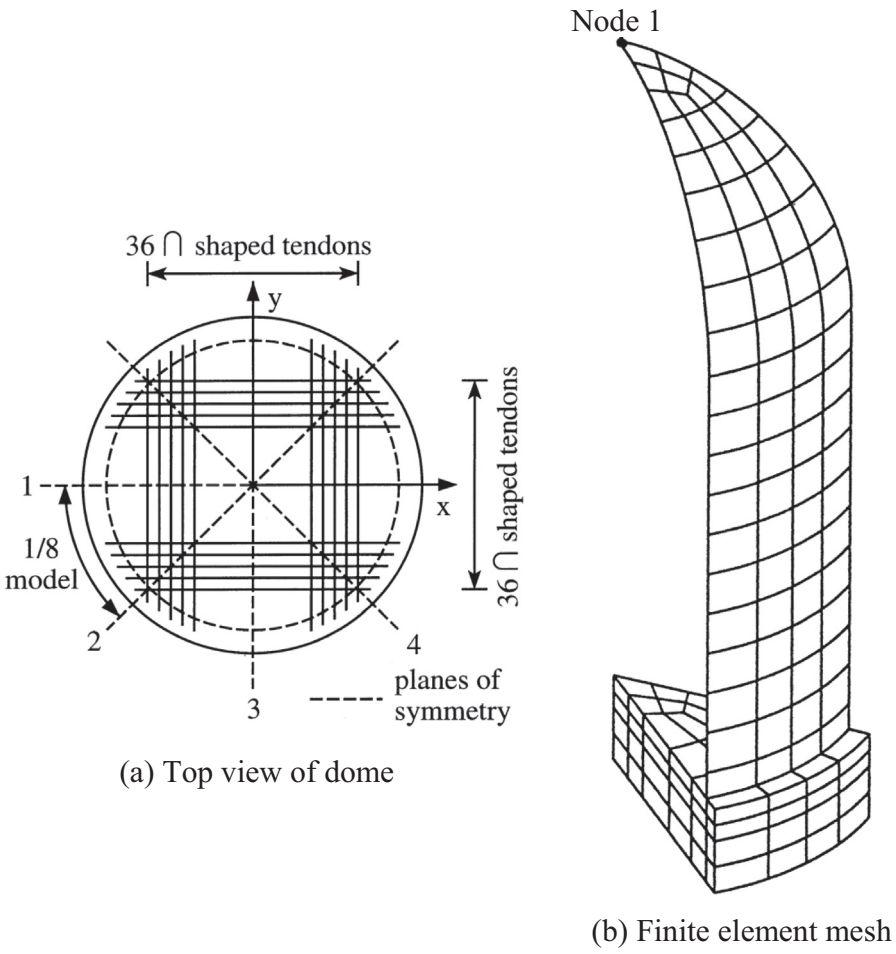

Fig. 2. 1/8 model of the PWR prestressed concrete containment of Maanshan nuclear power plant.

and these shear flexible shell elements can be used for both thick and thin shell analysis (Dassault Systèmes Corporation, 2014). At the bottom of the base slab, special purpose interface elements are used to link the base slab to the ground. The interface elements allow the contact surfaces between the base slab and the ground to remain closed or open but not to penetrate each other.

3. Material properties and constitutive models

The materials used in the containment can be divided into four groups, which are steel reinforcing bar, prestressing tendon, steel liner plate and concrete. The material properties of all the materials and their constitutive models used by Abaqus are briefly discussed in the following sections.

3.1. Steel reinforcing bar

The reinforcement used in the containment structure is ASTM A-615 Grade 60 steel with yield stress

$$\sigma_y = 414 \text{ MPa} \quad (1)$$

and its elastic modulus is assumed to be (ACI, 2011):

$$E_s = 200 \text{ GPa} \quad (2)$$

The stress–strain curve of the reinforcing bar is assumed to be elastic-perfectly plastic (Fig. 3).

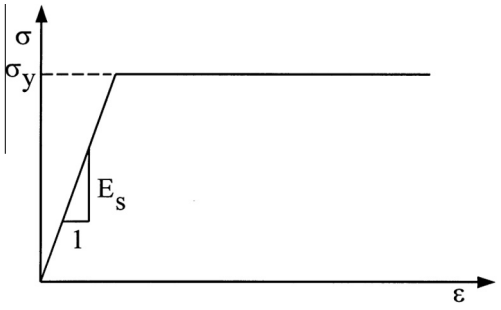

Fig. 3. Elastic perfectly plastic model for steel reinforcing bar and steel liner plate.

3.2. Steel liner plate

The yield stress of the liner plate is:

$$\sigma_y = 165 \text{ MPa} \quad (3)$$

In the analysis, the elastic modulus E_s and the Poisson's ratio v_s of both types of the steel liner plate are assumed to be:

$$E_s = 200 \text{ GPa} \quad (4)$$

$$v_s = 0.3 \quad (5)$$

The uniaxial behavior of the steel liner plate is similar to reinforcing bar and thus can be simulated by an elastic perfectly plastic model as shown in Fig. 3. When the liner plate is subjected to

biaxial stresses, a von Mises yield criterion $f(\sigma_1, \sigma_2)$ is employed to define the elastic limit (Fig. 4), where σ_1 and σ_2 are principal stresses and:

$$f(\sigma_1, \sigma_2) = \sqrt{\sigma_1^2 + \sigma_1^2 - \sigma_1\sigma_2} = \sigma_y \tag{6}$$

The response of the liner plate is modeled by an elastic-perfectly plastic theory with associated flow rule. When the stress points fall inside the yield surface, the behavior of the liner plate is linearly elastic. If the stresses of the liner plate reach the yield surface, the behavior of the liner plate becomes perfectly plastic. Consequently, the liner plate is assumed to fail and cannot resist any further loading.

3.3. Prestressing tendon

The prestressing tendon used in the containment is composed of thirty-seven Grade 270 strands. The diameter of each strand is 1.52 cm. The average tensile prestress is 1398 MPa in the meridian tendons and 1326 MPa in the circumferential tendons (Taiwan Power Company, 1981; Lin, 1997). Due to the lack of material test data, the nonlinear stress–stain curve of the strand given by Nilson and Winter (1991) is adopted and simplified to a piecewise linear curve as shown in Fig. 5. In addition, the elastic modulus of the tendon is assumed to be:

$$E_s = 190 \text{ GPa} \tag{7}$$

In Abaqus, the prestressing tendon and the steel reinforcement are treated as equivalent uniaxial materials, which are smeared through the element section. In order to properly model the constitutive behaviors of the tendon and the reinforcement, the cross sectional area, spacing, position and orientation of each layer of tendon or steel bar within each element need to be specified.

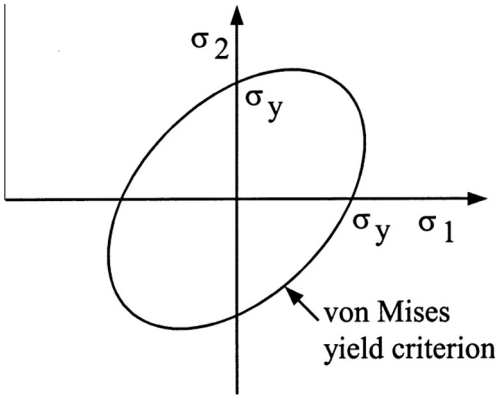

Fig. 4. von Mises yield criterion for steel liner plate.

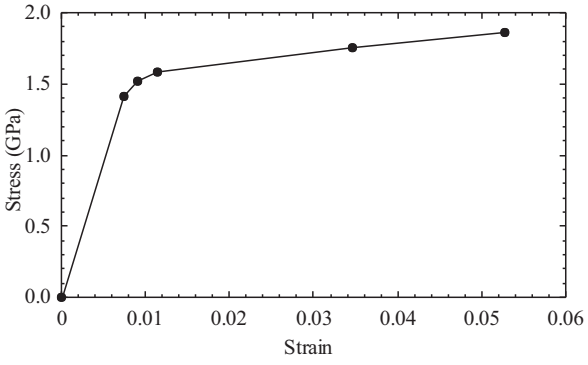

Fig. 5. Stress–strain curve for prestressing tendon.

3.4. Relaxation of the prestressing tendon

The relaxation model in Abaqus for the analysis of prestressing tendon is given by the following expression:

$$\sigma = \left[\sigma_o^{1-n} - \frac{A}{1+m}E(1-n)t^{1+m}\right]^{\frac{1}{1-n}} \tag{8}$$

where σ is the remaining stress of the prestressing tendon after relaxation, σ_o is the initial stress of the prestressing tendon, $E = E_s = 189.6$ GPa is the elastic modulus of the tendon, and t is time (unit in hour). We can then define a parameter R as the relaxation value in which:

$$R = \frac{\sigma_o - \sigma}{\sigma_o} = 1 - \frac{1}{\sigma_o}\left[\sigma_o^{1-n} - \frac{A}{1+m}E(1-n)t^{1+m}\right]^{\frac{1}{1-n}} \tag{9}$$

The constants A, m, n in Eqs. (8) and (9) are material dependent parameters. The values of these constants are determined by a curve fit to the experimental data tested in the period of 1000 h (Lin, 1997; Atomic Energy Council, 1995) and are listed below:

$$A = A_o = 3.054 \times 10^{-7} \tag{10a}$$

$$m = m_o = -0.8881 \tag{10b}$$

$$n = n_o = 0.5037 \tag{10c}$$

The plot of relaxation value R against time t (R–t curve) is shown in Fig. 6.

3.5. Concrete

The concrete used in the containment structure has a uniaxial compressive strength f_c' given as:

$$f_c' = 34.5 \text{ MPa} \tag{11}$$

Under uniaxial compression, the concrete strain ε_o corresponding to the peak stress f_c' is usually around the range of 0.002–0.003. A representative value is (ACI, 2011):

$$\varepsilon_o = 0.003 \tag{12}$$

The Poisson's ratio v_c of concrete under uniaxial compressive stress ranges from about 0.15 to 0.22, with a representative value of 0.19 or 0.20 (ASCE, 1982). In this study, the Poisson's ratio of concrete is assumed to be

$$v_c = 0.2 \tag{13}$$

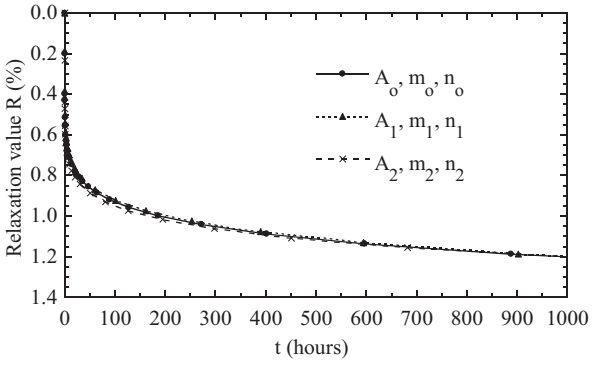

Fig. 6. Relaxation value R versus time t ($0 \leqslant t \leqslant 1000$ h).

The uniaxial tensile strength f_c' of concrete is difficult to measure and is normally taken as (ASCE, 1982):

$$f_t' = 0.33\sqrt{f_c'}\ \text{MPa} \tag{14}$$

The initial modulus of elasticity of concrete E_c is highly correlated to its compressive strength and can be calculated with reasonable accuracy from the empirical equation (ACI, 2011):

$$E_c = 4700\sqrt{f_c'}\ \text{MPa} \tag{15}$$

It should be noted that in Eqs. (14) and (15) the unit of f_c' is in MPa.

Under different combinations of loading, the failure strengths of concrete are different from that under uniaxial condition. However, the maximum strength envelope under multiple stress conditions seems to be largely independent of load path (Kupfer et al., 1969). In Abaqus, a Mohr-Coulomb type compression surface combined with a crack detection surface are used to model the failure surface of concrete (Fig. 7). When the principal stress components of concrete are dominantly compressive, the response of concrete is modeled by an elastic-plastic theory with associate flow and isotropic hardening rule. In tension, once cracking is defined to occur (by the crack detection surface), the orientation of the cracks is stored. Damaged elasticity is then used to model the existing cracks.

When plastic deformation occurs, there should be a certain parameter to guide the expansion of the yield surface. A commonly used approach is to relate the multidimensional stress and strain conditions to a pair of quantities, namely, the effective stress σ_c and effective strain ε_c, such that results obtained following different loading paths can all be correlated by means of the equivalent uniaxial stress–strain curve. The stress–strain relationship proposed by Saenz (1964) has been widely adopted as the uniaxial stress–strain curve for concrete and it has the following form:

$$\sigma_c = \frac{E_c\varepsilon_c}{1 + (R + R_E - 2)\left(\frac{\varepsilon_c}{\varepsilon_o}\right) - (2R-1)\left(\frac{\varepsilon_c}{\varepsilon_o}\right)^2 + R\left(\frac{\varepsilon_c}{\varepsilon_o}\right)^3} \tag{16}$$

where

$$R = \frac{R_E(R_\sigma - 1)}{(R_\varepsilon - 1)^2} - \frac{1}{R_\varepsilon}, \quad R_E = \frac{E_c}{E_o}, \quad E_o = \frac{f_c'}{\varepsilon_o}$$

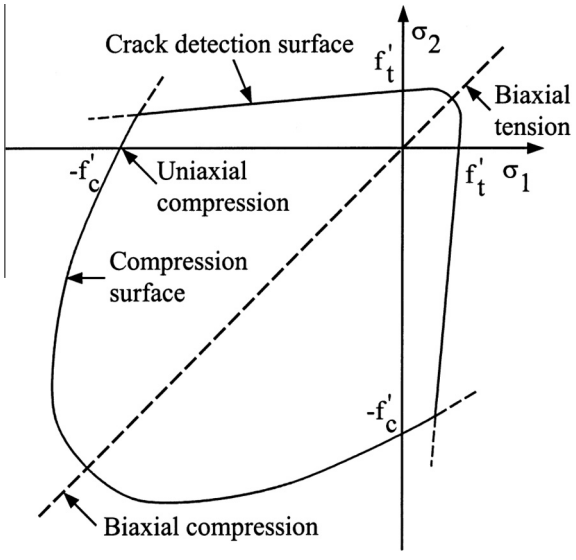

Fig. 7. Concrete failure surface in plane stress.

and $R_\sigma = 4,\ R_\varepsilon = 4$ may be used (Hu and Schnobrich, 1991). In the analysis, Eq. (16) is taken as the equivalent uniaxial stress–strain curve for concrete and approximated by several piecewise linear segments as shown in Fig. 8.

When cracking of concrete takes place, a smeared model is used to represent the discontinuous macro crack behavior. It is known that the cracked concrete of a reinforced concrete element can still carry some tensile stress in the direction normal to the crack, which is termed tension stiffening (ASCE, 1982). In this study, a simple descending line is used to model this tension stiffening phenomenon (Fig. 9). The default value of the strain ε^* at which the tension stiffening stress reduced to zero is (Dassault Systèmes Corporation, 2014):

$$\varepsilon^* = 0.001 \tag{17}$$

During the post cracking stage, the cracked reinforced concrete can still transfer shear forces through aggregate interlock or shear friction, which is termed shear retention (ASCE, 1982). Assume the shear modulus of intact concrete is G_c. The reduced shear modulus $\hat{G}$ of cracked concrete can be expressed as:

$$\hat{G} = \mu G_c \tag{18a}$$

and

$$\mu = 1 - \varepsilon/\varepsilon_{\max} \tag{18b}$$

where ε is the strain normal to the crack direction and $\varepsilon_{\max}$ is the strain at which the parameter μ reduces to zero (Fig. 10). In Abaqus, $\varepsilon_{\max}$ is usually assumed to be a very large value, i.e., $\mu = 1$ (full shear retention). In this investigation, other than specified, the default values for tension stiffening parameter $\varepsilon^* = 0.001$ and for shear retention parameter $\mu = 1$ are used.

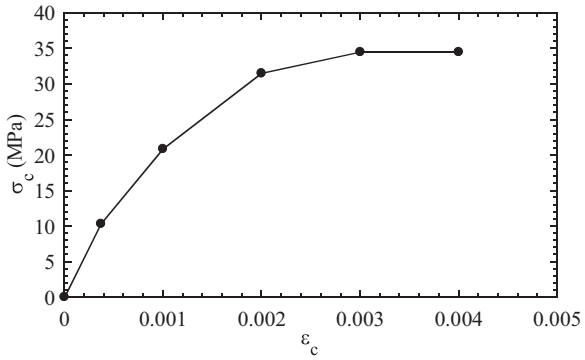

Fig. 8. Equivalent uniaxial stress–strain curve for concrete.

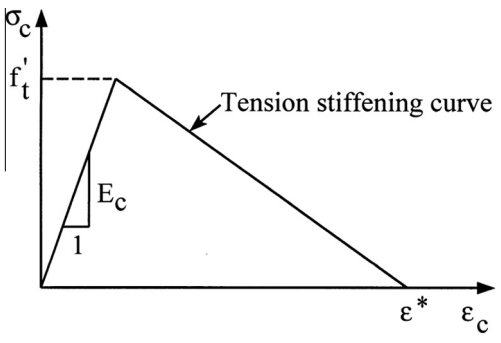

Fig. 9. Tension stiffening model.

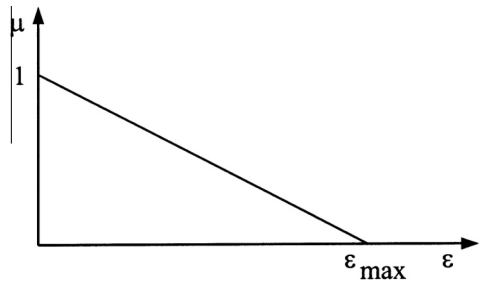

Fig. 10. Shear retention parameter.

4. Numerical analysis

4.1. Initial ultimate pressure capacity of containment

In this section, the initial ultimate pressure capacity of the containment is calculated as the referenced value for the relaxation analyses. The containment structure has a considerable amount of dead load contributed by reinforced concrete. In this investigation, it is assumed that the dead load, w_c, caused by the reinforced concrete is (Wang et al., 2007):

$$w_c = 2400\ \mathrm{kg/m^3} \tag{19}$$

In addition, a dead load of 15.58 MN due to equipment (Taiwan Power Company, 1981; Lin, 1997) is considered to be uniformly distributed to the top surface of the base slab. In the finite element analysis, those dead loads and the prestressing forces from the tendons are applied to the containment first. After the structure is in an equilibrium condition, the internal pressure p is then applied to the containment up to failure.

Fig. 11 shows the internal pressure p versus the displacement of node 1 (at the apex of the containment) in the z direction. The ultimate load p_u for the complete containment model is 761 kPa, which is about 58% higher than the design pressure 482 kPa. If the steel liner plate of the containment is not included in the model, the ultimate load becomes 752 kPa. If the dead load of the equipment is not considered, the ultimate load is 742 kPa. From this figure, it can be seen that all the curves are very close. The influences of the steel liner plate and the equipment load to the ultimate load of the containment are about 1–2.5%. Hence, for a rough estimation of the ultimate capacity of the containment, the steel linear plate and the equipment dead load may be neglected.

The deformation shape of the containment under the ultimate internal pressure condition is shown in Fig. 12a and the crack patterns of the concrete at the inner and outer sides of the containment are shown in Fig. 12b. From these figures we can observe that under the ultimate pressure, the base slab tends to lift. Most of the deformations take place in the dome. In addition, because of the stress concentration, cracks are likely to occur near the apex of the dome, the junction of the dome and cylinder, and the bottom of the cylinder.

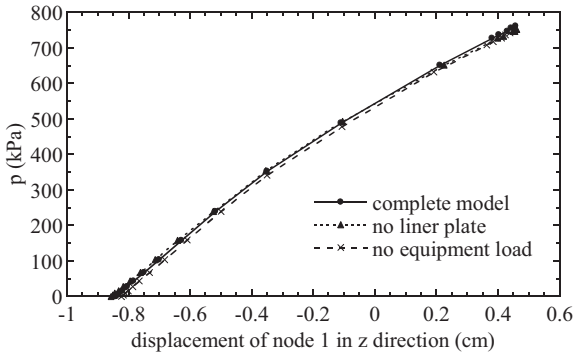

Fig. 11. Influence of equipment load and steel liner plate on the ultimate pressure capacity of containment.

4.2. Relaxation of prestressing tendons for the containment

In this section, long-term prestressing loss due to the relaxation of the prestressing tendons is studied and the aforementioned relaxation model for prestressing tendons is used in the finite element model.

Fig. 13a indicates the locations of the meridian tendons under investigation and Fig. 13b indicates the locations of the circumferential tendons under investigation. Fig. 14a shows the stresses of the meridian tendons at locations A, B, C, D and E on the containment versus time for the period of 40 years (about 350,000 h). It can be seen that these curves are very similar. The stresses in the meridian tendons at these locations lose significantly within the first 2 years (about 17,500 h). However, after the 2nd year, these stresses become more stable and do not change significantly. The average stress in the meridian tendons at these five locations loses about 11.1% at the end of the 1st year, 15.4% at the end of the 10th year, and 18.8% at the end of the 40th year.

Fig. 14b shows the stresses of the circumferential tendons at locations F, G, H, I, J and K on the containment versus time for the period of 40 years. It can be seen that these curves are very similar again. The stresses in the circumferential tendons at these locations lose significantly within the first 2 years. After the 2nd year, these stresses become more stable and do not change significantly. The average stress in the circumferential tendons at these six locations loses about 10.7% at the end of the 1st year, 15.5% at the end of the 10th year, and 18.8% at the end of the 40th year. From Fig. 14a and b, we can conclude that for the tendons in the containment the loss of prestress could be less than 19% for the service period of 40 years.

4.3. Ultimate pressure capacity of containment after the relaxation of prestressing tendons

When the loss of prestress in the containment is investigated, it becomes crucial to know the ultimate pressure capacity of the containment after the relaxation of prestressing tendons taking placing. Fig. 15 shows the ultimate pressure p_u of the containment versus time t (in years). It can be seen that the ultimate pressure capacities of the containment are all equal to 761 kPa when the time t is less than 40 years. In addition, the associated crack patterns of the containment are all similar to those shown in Fig. 12 (Lin, 1997) and are not duplicated here. Fig. 16 shows the internal pressure p versus the displacement of node 1 in the z direction for $t = 0$ and 40 years. After 40 years of relaxation, the prestresses of the tendons in the containment are reduced and the initial displacement ($p = 0$, $t = 40$) of the containment is smaller (in absolute value) than that with no prestress loss ($p = 0$, $t = 0$). When the internal pressure p is applied, these two containments would behave in the similar manner (especially in the elastic range) up to failure. Hence, these two curves are almost parallel.

If the service period of the containment structure can be extended from 40 years to 60 years, the ultimate pressure capacity of the containment would decrease a little amount to 756 kPa. However, it is still 57% higher than the design pressure 482 kPa. Hence, it can be concluded that during the service period, the ultimate pressure capacity of the containment would not change with time, even the relaxation of prestressing tendons taking place.

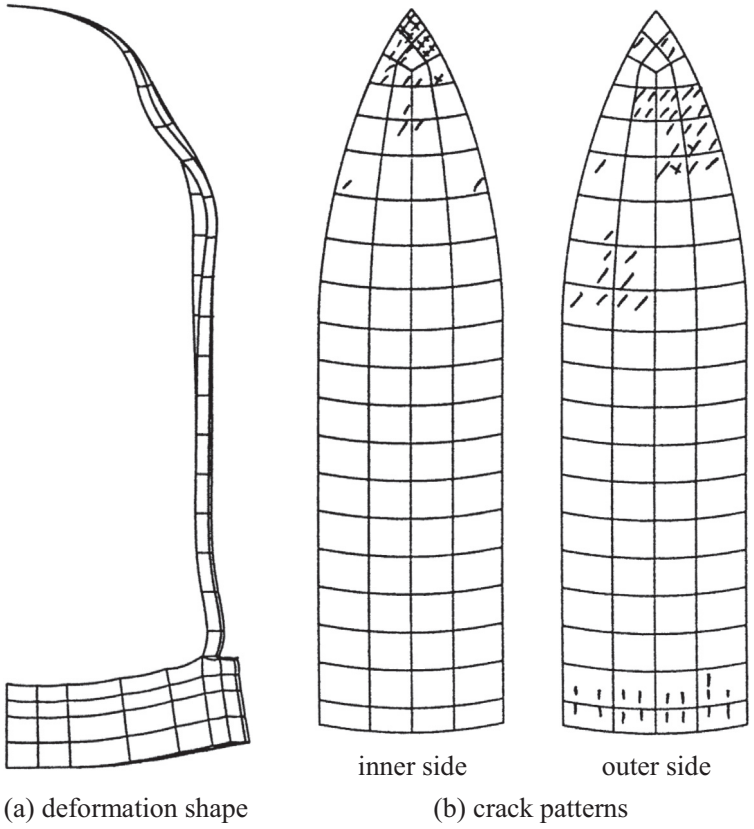

Fig. 12. Deformation shape and crack patterns of the containment under the ultimate internal pressure $p_u = 761$ kPa.

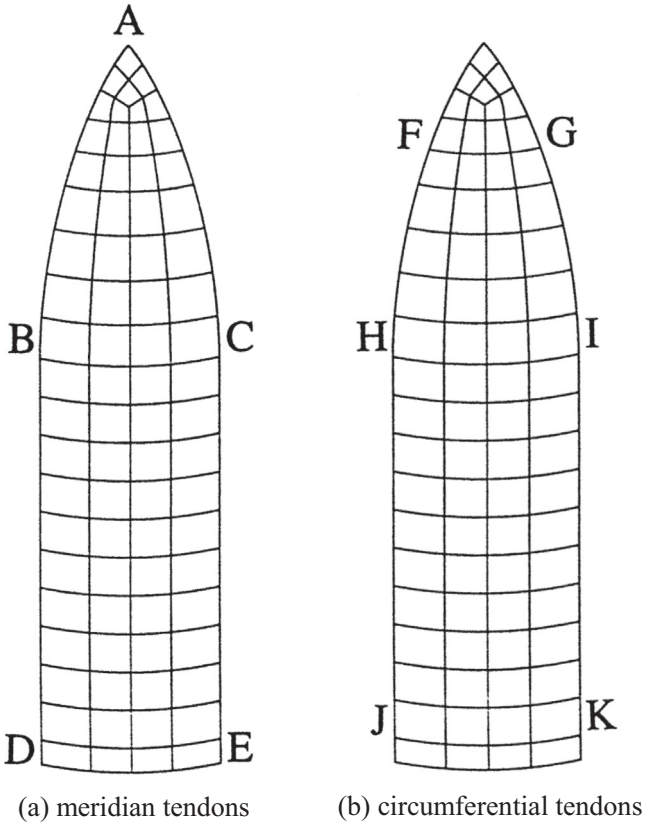

Fig. 13. Positions of tendons under investigation.

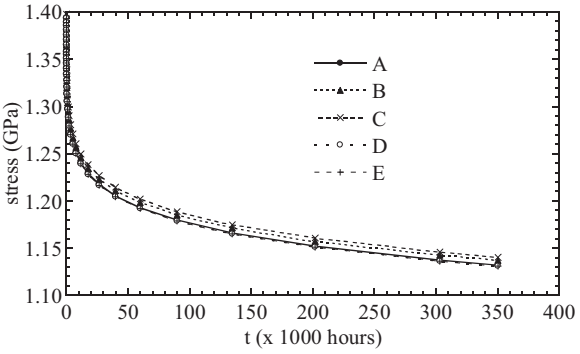

(a) stresses of the meridian tendons at locations A, B, C, D and E

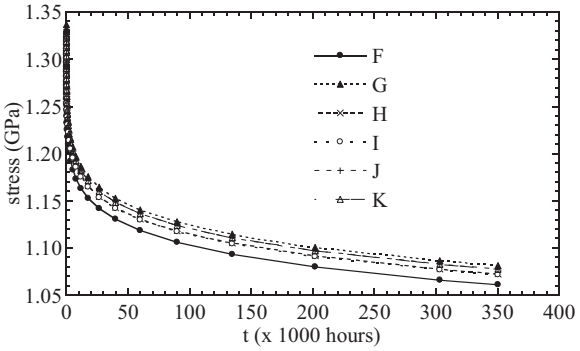

(b) stresses of the circumferential tendons at locations F, G, H, I, J and K

Fig. 14. Stress relaxations of the tendons in the containment.

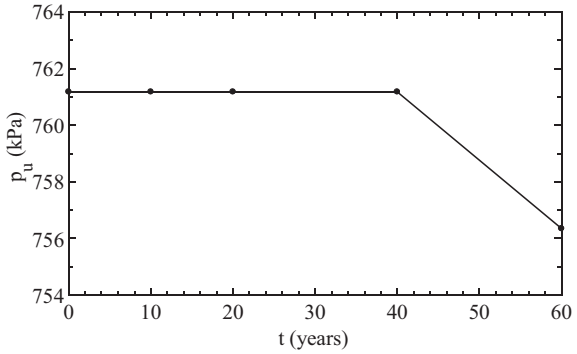

Fig. 15. Ultimate pressure capacity of containment versus time.

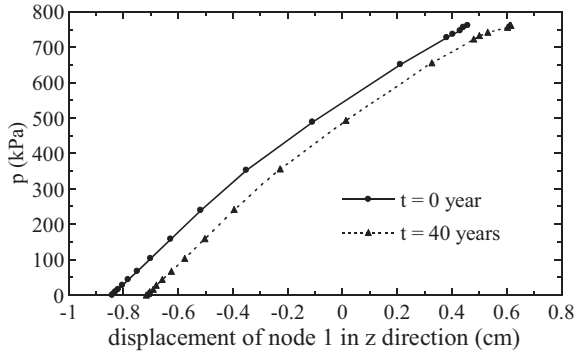

Fig. 16. Internal pressure p versus displacement of node 1 in z direction for $t = 0$ and 40 years.

4.4. Influence of initial prestress in the tendons on the ultimate pressure capacity of containment

In this section, the influence of initial prestress in the tendons on the ultimate pressure capacity of the containment is investigated. Since the relaxation of prestressing tendons does not affect the ultimate pressure capacity of the containment, the loss of prestress in the containment due to time effect is not considered in this section. The following analyses are based on the condition $t = 0$ year.

Let P_o represent the initial prestress being 1398 MPa in the meridian tendons and 1326 MPa in the circumferential tendons. Then nP_o means the initial prestress being n × 1398 MPa in the meridian tendons and n × 1326 MPa in the circumferential tendons. Fig. 17 shows the ultimate pressure capacity of the containment when the initial prestresses in the tendons are $0P_o$, $0.5P_o$, $0.67P_o$, $0.82P_o$, P_o and $1.2P_o$. When $n = 0$ (no initial stress), the containment becomes a reinforced concrete structure. As the result, the ultimate pressure capacity of the containment is very low and is equal to 192 kPa. When $n < 0.82$, it seems that the ultimate pressure capacity of the containment increases linearly with the increasing of n. However, when $0.82 \leqslant n \leqslant 1$, the ultimate pressure capacity of the containment becomes a constant value 761 kPa. When $n > 1$, the ultimate pressure capacity of the containment starts to decrease. When $n = 1.2$, the ultimate pressure capacity of the containment is 756 kPa. From this figure, we can conclude that proper prestresses in the tendons are important. Too low prestresses or too high prestresses in the tendons would reduce the ultimate pressure capacity of the containment.

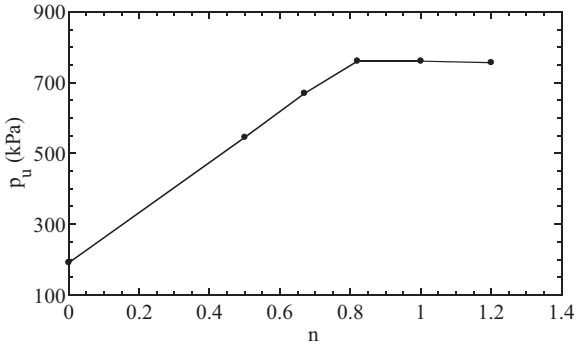

Fig. 17. Influence of initial prestress in the tendons on the ultimate pressure capacity of containment.

4.5. Influence of tendon relaxation curve on the ultimate pressure capacity of containment

The material dependent parameters A, m, n in Eqs. (8) and (9) are determined by a curve fit to experimental data tested in the period of 1000 h (Lin, 1997; Atomic Energy Council, 1995). In the previous analyses, these parameters are all selected to be:

$$A = A_o = 3.054 \times 10^{-7}$$
$$m = m_o = -0.8881$$
$$n = n_o = 0.5037$$

However, we can also select three arbitrary experimental data points on the relaxation value R versus time t curve (R–t curve) and solve for A, m and n using Eq. (9). If the data points at $t = 0$, 50 and 1000 h are selected, we can obtain:

$$A = A_1 = 3.129 \times 10^{-7}$$
$$m = m_1 = -0.8846$$
$$n = n_1 = 0.5$$

If the data points at $t = 0$, 200 and 1000 h are selected, we can obtain:

$$A = A_2 = 3.029 \times 10^{-7}$$
$$m = m_2 = -0.8985$$
$$n = n_2 = 0.5$$

The R–t curves simulated by these three sets of parameters are shown in Fig. 6. It can be seen that these three curves are almost identical. However, when the time is increased from 1000 h to 40 years, these R–t curves do have some difference as shown by Fig. 18.

Fig. 19a shows the average stress of the meridian tendons at locations A, B, C, D and E on the containment versus time for the

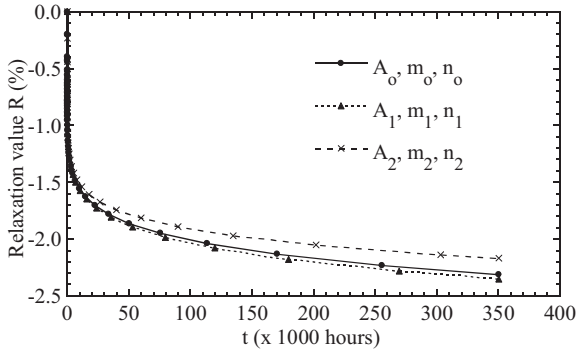

Fig. 18. Relaxation value R versus time t ($0 \leqslant t \leqslant 40$ years).

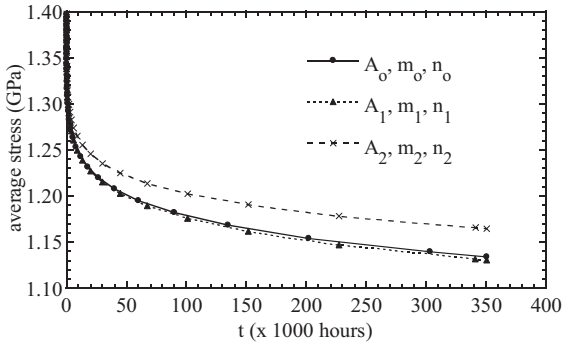

(a) average stress of the meridian tendons at locations A, B, C, D and E

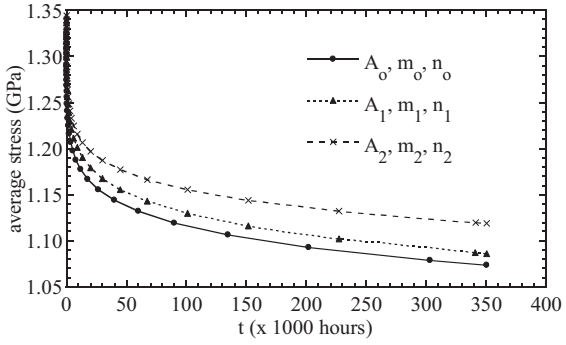

(b) average stress of the circumferential tendons at locations F, G, H, I, J and K

Fig. 19. Influence of different *R–t* curves on the stress relaxations of the tendons in the containment.

period of 40 years, calculated by using different *R–t* curves. Fig. 19b shows the average stress of the meridian tendons at locations F, G, H, I, J and K on the containment versus time for the period of 40 years, also calculated by using different *R–t* curves. These numerical results are also summarized in Tables 1 and 2. At the end of the 40th year, when parameters A_o, m_o, n_o are used, the predicted average stress in the meridian tendon would lose 18.9% and the predicted average stress in the circumferential tendon would lose 18.9%. When parameters A_1, m_1, n_1 are used, the predicted average stress in the meridian tendon would lose 19.1% and the predicted average stress in the circumferential tendon would lose 18.1%. When parameters A_2, m_2, n_2 are used, the predicted average stress in the meridian tendon would lose 16.7% and the predicted average stress in the circumferential tendon would lose 15.6%. Though the predicted stresses by using these three sets of parameters are different, these differences are not significant. It seems reasonable to conclude that the stress loss of the tendon in the containment would not exceed 20% at the end of the 40-year service period.

Comparing Tables 1 and 2 with Fig. 18, we can find that the stress loss of tendons in the containment (say 15%∼19%) at the end of the 40th year is much greater than that for a single experimental tendon at laboratory (say 2.4%) at the end of the 40th year.

Table 3 shows the ultimate pressure capacity of the containment calculated by using different sets of parameters. From this table, we can see that the ultimate pressure capacities of the containment at the end of the 40th year are all the same and equal to the initial ultimate pressure capacities of the containment. Hence, it can be concluded that the ultimate pressure capacity of the containment calculated by using different relaxation curves would be the same at the end of the service period.

4.6. Influence of tension stiffening on the ultimate pressure capacity of containment

Fig. 20 shows the internal pressure–displacement curves of node 1 in the *z* direction at the end of the 40th years, which are obtained by using different tension stiffening parameter ε^* (Fig. 9). It seems that these curves are almost the same. The only difference is that the ultimate pressure capacity of the containment is 757 kPa when $\varepsilon^* = 0.0005$, and is 761 kPa when $\varepsilon^* = 0.001$ or 0.002. Hence, as long as tension stiffening is properly taken into consideration, the influence of tension stiffening parameter on the ultimate pressure capacity of the containment under long-term prestressing loss may not be significant.

4.7. Influence of shear retention on the ultimate pressure capacity of containment

Fig. 21 shows the internal pressure–displacement curves of node 1 in the *z* direction at the end of the 40th years, which are

Table 3
Ultimate pressure capacity of containment calculated by using different sets of parameters.

Parameters	Initial ultimate pressure capacity of containment at t = 0 year (kPa)	Ultimate pressure capacity of containment at t = 40 years (kPa)
A_o, m_o, n_o	761	761
A_1, m_1, n_1	761	761
A_2, m_2, n_2	761	761

Table 1
Average stress of the meridian tendons at locations A, B, C, D and E on the containment predicted by different *R–t* curves.

Parameters	Initial stress (GPa)	End of 1st year		End of 10th year		End of 40th year	
		Stress (GPa)	Stress loss (%)	Stress (GPa)	Stress loss (%)	Stress (GPa)	Stress loss (%)
A_o, m_o, n_o	1.398	1.242	11.2	1.182	15.5	1.134	18.9
A_1, m_1, n_1		1.250	10.6	1.182	15.5	1.131	19.1
A_2, m_2, n_2		1.265	9.5	1.208	13.6	1.165	16.7

Table 2
Average stress of the circumferential tendons at locations F, G, H, I, J and K on the containment predicted by different *R–t* curves.

Parameters	Initial stress (GPa)	End of 1st year		End of 10th year		End of 40th year	
		Stress (GPa)	Stress loss (%)	Stress (GPa)	Stress loss (%)	Stress (GPa)	Stress loss (%)
A_o, m_o, n_o	1.326	1.183	10.8	1.120	15.5	1.076	18.9
A_1, m_1, n_1		1.201	9.4	1.136	14.3	1.086	18.1
A_2, m_2, n_2		1.216	8.3	1.161	12.4	1.119	15.6

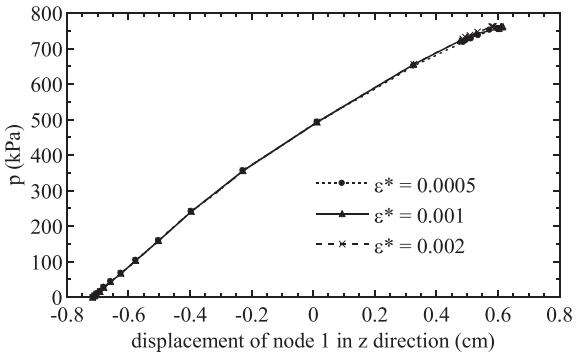

Fig. 20. Influence of tension stiffening on the ultimate pressure capacity of containment under long-term prestressing loss.

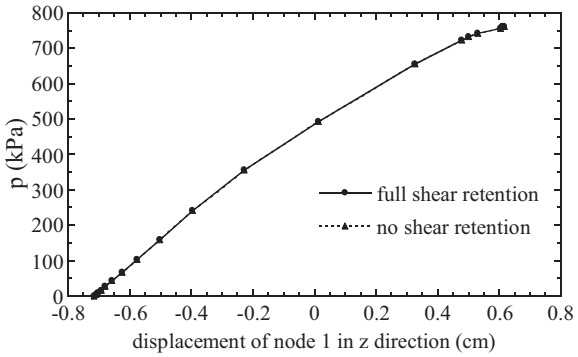

Fig. 21. Influence of shear retention on the ultimate pressure capacity of containment under long-term prestressing loss.

obtained by using full shear retention and no shear retention. For full shear retention, the parameter μ is equal to 1 (Eq. (18a)), and the shear modulus of cracked concrete is assumed to be the same as that of intact concrete. For no shear retention, the parameter μ is set to 0, and the shear modulus of cracked concrete is assumed to be zero. From this figure we can see that the internal pressure–displacement curves of these two extreme conditions are almost the same. In addition, the ultimate pressure capacities of the containments for these two cases are the same and equal 761 kPa. Hence, it can be concluded that shear retention has very little influence on the ultimate pressure capacity of the containment under long-term prestressing loss.

5. Conclusions

From the ultimate analysis of PWR prestressed concrete containment at Maanshan nuclear power plant under long-term prestressing loss, the following conclusions may be drawn:

(1) The initial ultimate pressure capacity of the containment is 761 kPa, which is about 58% higher than the design pressure of 482 kPa. Under the ultimate pressure condition, cracks are likely to occur near the apex of the dome, the junction of the dome and cylinder, and the bottom of the cylinder.
(2) For the tendons in the containment, the loss of prestress could be less than 19% for the service period of 40 years.
(3) During the service period, the ultimate pressure capacity of the containment would not change with time, even the relaxation of prestressing tendons taking place.
(4) Proper prestresses in the tendons are important. Too low prestresses or too high prestresses in the tendons would reduce the ultimate pressure capacity of the containment.
(5) The stress loss of the tendon in the containment would not exceed 20% at the end of the 40-year service period.
(6) The stress loss of tendons in the containment is much greater than that for a single experimental tendon at laboratory
(7) As long as tension stiffening is properly considered, the influence of tension stiffening parameter on the ultimate pressure capacity of the containment under long-term prestressing loss may not be significant.
(8) Shear retention has very little influence on the ultimate pressure capacity of the containment under long-term prestressing loss.

Acknowledgment

This research work was financially supported by the Atomic Energy Council of the Republic of China under Grant 862001NRD107.

References

Abaqus, Inc., Failure of a prestressed concrete containment vessel, Abaqus Technology Brief, TB-03-PCCV-1, Providence, Rhode Island, 2007.
ACI Committee 318, 2011. Building Code Requirements for Structural Concrete (ACI 318-11) and commentary, American Concrete Institute, Farmington Hills, Michigan.
Amin, M., Eberhardt, A.C., Erler, B.A., 1993. Design considerations for concrete containments under severe accident loads. Nucl. Eng. Des. 145, 331–338.
Andreoli, V., Angeloni, P., Contri, P., Brusa, L., 1993. Numerical simulation of the ultimate load capacity of a reactor containment building. Nucl. Eng. Des. 145, 403–417.
Argyris, J.H., Gaust, G., Szimmat, J., Warnke, E.P., Willam, K.J., 1974. Recent developments in the finite element analysis of prestressed concrete reactor vessels. Nucl. Eng. Des. 28, 42–75.
ASCE Task Committee on Concrete and Masonry Structure, State of the Art Report on Finite Element Analysis of Reinforced Concrete, ASCE, 1982.
Ashar, H., Costello, J., Graves, H. Prestress force losses in containments of U.S. Nuclear Power Plants, NEA/CSNI/R(97)9, Joint WANO/OECD-NEA workshop on Prestress loss in NPP containments organized by EDF/IPSN, Civaux NPP, France, August 25–26, 1997, pp. 337–356.
Atomic Energy Council, Nuclear Regulatory Division, 1995. Testing of Civil Structures for Nuclear Engineering Applications (in Chinese).
Basha, S.M., Singh, R.K., Patnaik, R., Ramanujam, S., Kushwaha, H.S., Venkat Raj, V., 2003. Predictions of ultimate load capacity for pre-stressed concrete containment vessel model with BARC finite element code ULCA. Ann. Nucl. Energy 30 (4), 437–471.
Boeck, B.D., 1993. A review of containment accidents. Nucl. Eng. Des. 145, 279–288.
Borri, A., Sorace, S., 1993. FE analysis strategies for structural materials with small tensile strength. J. Press. Vessels Technol. (ASME) 115, 156–163.
Chen, W.F., 1982. Plasticity in Reinforced Concrete. McGraw-Hill.
Connor, J.J., Sarne, Y. Nonlinear analysis of prestressed concrete reactor pressure vessels, in: Third international conference on structural mechanics in reactor technology, London, U.K., September 1–5, 1975, Vol. 3, H2/2.
Cornish-Bowdena, I., Thillard, G., Capra, B. Prediction of prestressing losses for long term operation of nuclear reactor buildings, EPJ Web of Conferences 12, 04002, 2011.
Dassault Systèmes Corporation, SIMULIA Abaqus Analysis User's Manuals, Theory Manuals and Example Problems Manuals, Version 6.14, France, 2014.
Goodpasture, D.W., Burdette, E.G., Callahan, J.P., 1978. Design and analysis of multicavity prestressed concrete reactor vessels. Nucl. Eng. Des. 46, 81–100.
Hu, H.-T., Liang, J.I., 2000. Ultimate analysis of BWR Mark III reinforced concrete containment subjected to internal pressure. Nucl. Eng. Des. 195 (1), 1–11.
Hu, H.-T., Lin, Y.-H., 2006. Ultimate analysis of PWR prestressed concrete containment subjected to internal pressure". Int. J. Press. Vessels Pip. 83 (3), 161–167.
Hu, H.-T., Schnobrich, W.C., 1989. Constitutive modelling of concrete by using nonassociated plasticity. J. Mater. Civil Eng. (ASCE) 1 (4), 199–216.
Hu, H.-T., Schnobrich, W.C., 1990. Nonlinear analysis of cracked reinforced concrete. ACI Struct. J. 87 (2), 199–207.
Hu, H.-T., Schnobrich, W.C., 1991. Nonlinear finite element analysis of reinforced concrete plates and shells under monotonic loading. Comput. Struct. 38, 637–651.
Kupfer, H., Hilsdorf, H.K., Rusch, H., 1969. Behavior of concrete under biaxial stresses. ACI J. 66, 656–666.
Lin, J.-X. Creep analysis of PWR Prestressed Concrete Containment. (MS thesis) (in Chinese), Department of Civil Engineering, National Cheng Kung University, Tainan, Taiwan, R.O.C., 1997.
Maliavine, V.P., Prestress losses in containment of VVER 1000 units, Joint WANO/OECD-NEA workshop on Prestress loss in NPP containments organized by EDF/IPSN, Civaux NPP, France, August 25–26, 1997, pp. 205–220.

Martinent, E., Guinet, P., Rousselle, H., Granger, L. Prestress losses in NPP containments – The EDF experience, Joint WANO/OECD-NEA workshop on Prestress loss in NPP containments organized by EDF/IPSN, Civaux NPP, France, August 25–26, 1997, pp. 95–114.

Meyer, C., Okamura, H., 1985. Finite Element Analysis of Reinforced Concrete Structures. ASCE.

Nilson, A.H., Winter, G., 1991. Design of Concrete Structures, eleventh ed. McGraw-Hill.

Patel, S.C., Gupchup, V.N., Basu, P.C., Shylamoni, P. Impact of loss of prestressing force on NPP containment structure, paper #H04/4, 19th International Conference on Structural Mechanics in Reactor Technology (SMiRT), Toronto, Canada, August 12–17, 2007.

Pfeiffer, P.A., Kennedy, J.M., Marchertas, A.H., 1992. Post-test analysis for the nonlinear response of an internally pressurized one six scale reinforced concrete containment model. Nucl. Eng. Des. 133, 143–157.

Saenz, L.P., 1964. Discussion of "Equation for the stress–strain curve of concrete" by Desayi, P., Krishnan, S. ACI J. 61, 1229–1235.

Saito, H., Muramatsu, Y., Furukawa, H., Hasegawa, T., Mutoh, A., 1993. Post-test of a 1:10-scale top slab model of ABWR/RCCV subjected to internal pressure. Nucl. Eng. Des. 145, 339–353.

Smith, J.A. Capacity of Prestressed Concrete Containment Vessels with Prestressing Loss, Sandia Report, SAND2001-1762, Sandia National Laboratories, Albuquerque, New Mexico, 2001.

Taiwan Power Company, Final Safety Analysis Report, Maanshan Nuclear Power Station Units 1 and 2, Vol. 5, 1981.

U.S. Nuclear Regulatory Commission, Office of Nuclear Reactor Regulation. Standard Review Plan for the Review of Safety Analysis Reports for Nuclear Plants, Section 3.8.1, NUREG-0800, 1987.

U.S. Nuclear Regulatory Commission, Office of Nuclear Reactor Regulation. Determining Prestressing Forces for Inspection of Prestressed Concrete Containments, Regulatory Guide 1.35.1, 1990.

Wang, C.-K., Salmon, C.G., Pincheira, J.A., 2007. Reinforced Concrete Design, seventh ed. John Wiley and Sons (Chapter One).